Transport in Porous Media (2007) 68:107–127
DOI 10.1007/s11242-006-0005-0

The Local Geometry of Gas Injection into Saturated Homogeneous Porous Media

JOHN S. SELKER[1,*], MICHAEL NIEMET[2], NORTON G. MCDUFFIE[3], STEVEN M. GORELICK[4] and JEAN-YVES PARLANGE[5]

[1]*Department of Biological and Ecological Engineering, Oregon State University, Corvallis, OR, USA*
[2]*CH2M HILL, Corvallis, OR, USA*
[3]*Consultant, Corvallis, OR, USA*
[4]*Department of Geological and Environmental Sciences, Stanford University, Stanford, CA, USA*
[5]*Department of Biological and Environmental Engineering, Cornell University, Ithaca, NY, USA*

(Received: 10 March 2005; accepted in final form: 9 January 2006)

Abstract. The injection of gases into liquid saturated porous media is of theoretical and practical interest (e.g., air sparging for the removal of volatile organic compounds from contaminated aquifer sediments). The influence of the rate of gas delivery and the vertical distance from the source are developed. The concept of a "near-injection region" is presented in which the pressure gradients exceed buoyant gradients and thus exhibits largely radial flow. The near-injection size is shown to have an area required to carry the injected gas flow under unit gradient. The parabolic movement of gas outside of this area which has often been observed is explained as reflecting the sum of many realizations of gas channels following random lateral movements as they precede upward independent of flux. These concepts are confirmed through comparison with published and experimental data of air injection into slabs consisting of saturated sands of a range of textures.

Key words: gas flow, gas sparging, fingered flow, bouyant flow, capillary number, bond number.

Variables Employed

A the area through which flow is passing
A_{ug} the cross sectional area of gas flow under unit gradient flow
a the width of an ellipsoid
b the depth of an ellipsoid
B_0 the Bond Number

*Present address: Department of Bioengineering, rm 210 Gilmore Hall, Oregon State University, Corvallis, OR 97331-3609, USA; Tel.: 541-737-6304; Fax: 541-737-2082; e-mail: selkerj@engr.orst.edu

B_0^* the modified Bond Number, defined to be B_0/α.
c the circumference of an ellipse.
C_a the Capillary Number.
F_b the buoyant force on the hemispheric invasion front of a channel.
g the acceleration of gravity.
P the pressure at a point.
P_c the capillary pressure required for invasion of a pore.
q the specific flux.
Q the flux of invading fluid.
R the channel radius.
r the characteristic pore size of the medium.
s the surface area of an ellipsoid of rotation about its minor axis.
S the volume per unit length, of a channel of gas.
S_D the standard deviation of lateral channel displacement.
T the thickness of a two-dimensional flow cell.
v the characteristic velocity of the invasion front.
α the ratio of the mean pore neck to pore body diameter.
γ the solid–gas–liquid contact angle.
κ the intrinsic permeability of the medium.
κ_{sg} the intrinsic permeability at gas saturation.
μ the dynamic viscosity (resident or invading indicated by context).
$\Delta\rho$ the difference in density between the resident and invading fluids.
σ the interfacial energy (surface tension) between resident and invading fluids.
θ_g the gas-filled volume fraction.

1. Introduction

The study of gas movement following injection into liquid saturated porous media is an active area of exploration for theoretical and practical reasons (e.g., Lohse, 2003; Krauss *et al.*, 2003). The injection of gases below the water table in sedimentary aquifer materials, or sparging, is a method commonly employed to reduce contamination with volatile compounds (e.g., Reddy *et al.*, 1999; Lazik *et al.*, 2002; Reddy and Tekola, 2004), and has been proposed as a method to emplace trapped gas to promote biological processes and to reduce permeability (e.g., Fry *et al.*, 1997; Dror *et al.*, 2004). There have been several very useful articles devoted to observational study of the geometry of gas invasion in sandy materials in homogeneous materials (e.g., Clayton, 1998; Elder and Benson, 1999; Roosevelt and Corapcioglu, 1998). Our objectives are to present a physically based framework for the understanding the geometric features of a gas phase injected into a non-deforming homogeneous sandy material, and to validate these concepts with experimental data.

Although throughout this paper we use the image of an invading gas into an otherwise liquid filled system, most of the ideas presented would apply to other immiscible liquid invasion in porous media with contrasting density, though care would need to be taken with respect to non-zero

contact angle effects. In the groundwater literature this would include vertical upward invasion of a gasoline leak below a water table, or vertical downward invasion of a chlorinated solvent into an aquifer (e.g., Conrad *et al.*, 1992; Baldwin and Gladden, 1996; Imhoff *et al.*, 1994).

For slow invasion of a non-wetting fluid into a wetting-fluid in saturated porous media under the influence of gravity, it is useful to characterize the flow regime using the Bond number, B_0

$$B_0 = \frac{\Delta\rho g r^2}{\sigma}, \tag{1}$$

where $\Delta\rho$ is the difference in density between the resident and invading fluids; g is the acceleration of gravity; r is the characteristic pore size of the medium; and, σ is the interfacial energy (surface tension) between resident and invading fluids. To account for the influence of the pore-size distribution of the medium on gas movement, a modified Bond number B_0^* was presented by Brooks *et al.* (1999). B_0^* is defined to be B_0 divided by the ratio of the pore neck to pore body diameter (α), which ranges from 0.05 to 0.5. Using B_0^*, Brooks *et al.* (1999) classified flow into three regimes: *channel flow* for $B_0^* < 1$; *transition flow* for $1 < B_0^* < 3$; and *bubble flow* for $B_0^* > 3$.

For media with constant α near the upper limit (≈ 0.5), Frette *et al.* (1992) explored the scaling characteristics of non-wetting invasion with B_0, between 0.05 and 10. Frette *et al.* used the displaced volume per unit length, S, of a channel of invading low-density fluid as their primary metric. For $B_0 < 0.03$ (modified $B_0^* < 0.06$), S increases without limit; for $0.03 < B_0 < 0.3$ S scales with $B_0^{-0.7}$; while for $B_0 > 0.3$ the viscosity of their sugar solution was no longer negligible and considerations beyond Bond number would be required to interpret the resulting flow. These results were expanded upon by Chaouche *et al.* (1994), where the width of channels was used as a metric [proportional to the square root of the volume per length reported by Frette *et al.* (1992)]. The width was found to scale with $B_0^{-0.47}$ over the same narrow $0.03 < B_0 < 0.3$. In this same range of Bond numbers, Hirsch and Thompson (1994) found the width of fractal invasion patterns scaled with $B_0^{-0.47}$. For $0.03 < B_0 < 0.3$, gas has been observed to follow channels with ever-increasing numbers of lateral pores invaded for the channel to grow, but always with individual pores (rather than many pores) linking sequential vertical sections of the channel. In essence, the processes observed are still fundamentally buoyant forces favoring upward growth at each pore, but with the trend that direct upward invasion lessens for media with smaller pores because capillary forces are more dominant over buoyant forces, leading to more lateral pores filled.

When pore size crosses the threshold of $B_0 < 0.03$ channels become macroscopic forms in which individual pores no longer predominate as links between sections. In sand-sized porous media it was noted experimentally

by Ji *et al.* (1993) that gas moved in channels rather than either as discrete bubbles or in connected dendritic networks of pores. In addition, Ji *et al.* (1993) noted a parabolic shape to the gas plumes as they grew upward from the source. These results were followed by those of Hein *et al.* (1997); Clayton (1998); Semer *et al.* (1998); Brooks *et al.* (1999); Elder and Benson (1999); Lazik *et al.* (2002), and Krauss *et al.* (2003), among others, who also observed similar macro-channel behavior. Of these publications, Brooks *et al.* (1999) discussed the threshold between dendritic and channel behavior, but only to the extent that "a multipore analysis may then seem more appropriate than the single pore analysis presented earlier (in the paper)". Here we reconsider the physics and geometric controls that apply to these channels of gas flow, and find that the invasion phenomena are in some sense much simpler than those occurring at higher Bond number where pore size, and pore size distribution, must be included in the analysis. This paper focuses on identification of the sequential stages of development of an injected gas plume in water-saturated homogeneous sand, and provides a simple physical conceptual model to understand the experimental observations made by out team as well as selected studies from the literature.

2. Conceptual Framework

The capillary pressure, P_c, required to invade a pore is dictated by the effective size of the aperture leading to that pore (the pore throat) is given by the familiar Young–Laplace equation

$$P_c = \frac{2\sigma \cos \gamma}{r}, \tag{2}$$

where σ is the gas–liquid surface tension, γ is the solid–gas–liquid contact angle, and r is the effective radius of the characteristic aperture. For gas to invade a water filled pore it must overcome P_c. Each gas displacement will be directed by the opportunity to go in the path of most ready energy dissipation, which will correspond to the pore with the greatest aperture at the point where the gas has highest pressure. In the case of invading gas, generally this will involve an incremental advancement at the upper tip of a gas channel, in a random non-downward direction.

Gas invasion of a porous medium requires that a sequence of pores be drained, and the *relative* values of P_c for adjacent pores are central to the determination of which pore will be next invaded from a given gas-filled source. A separate consideration is the mean magnitude of the pressure required to obtain gas invasion. For gas invading water filled sands this pressure, stated in the convenient units of head, is typically on the order of 5 cm (e.g., Culligan *et al.*, 2000). Given our interest here in gross behavior

of buoyant gas invasion over meters of vertical travel, this initiation pressure is negligible compared to the pressure required to inject the air deeply below the zero-pressure water table for our case.

2.1. PORE-SCALE: BUOYANT CHANNELS

Our first objective is to compute the expected radius of a channel of gas rising through porous media (Figure 1). It is a remarkable fact that for finer media, with B_0 less than 0.01, that gas invasion occurs in the form of channels of gas flow as opposed to the dentridic patterns seen in coarser media (e.g., Frette *et al.*, 1992; Xu *et al.*, 1998). It is edifying to consider physically why this is true. At these low Bond numbers the capillary pressures are great compared to the gradients in buoyant forces between vertically adjacent pores, so in any pore or set of adjacent pores the invading fluid movements will be largely unaffected by buoyancy, which suggests the development of a patches of invaded pores that do not exhibit the effects of gravity. Eventually, however, this patch grows, and coalesces to form a zone of de-saturated pores across which the buoyant energy gradient is comparable to the capillary forces. This void space is pressurized sufficiently to continue expanding into additional space, but now vertical expansion can take place as a unified channel of connected gas-filled pores that sweeps across many pores as it grows. In sparging experiments the flow rates are typically high at the source, in which case viscous forces are significant, and a simple Bond Number analysis would be inappropriate. Far from the source, however, channels are formed primarily due to buoyant forcing being constrained by capillary entry pressures, where the Bond Number is appropriately applied. This flux-independence was evident in our experiments wherein many of the channels developed very slowly (often less than 1 cm/per minute), but in every case ultimately were indistinguishable from the more rapidly formed siblings.

To obtain an estimate of the channel diameter we assume a simple geometry of a cylindrical channel with a hemispheric upper termination. The upward growth of the plume is driven by the buoyancy of the upper hemispherical volume, and restrained by the surface tension exerted on the hemisphere about its perimeter. We expect growth when the forces are balanced. The buoyant force, F_b, on the hemisphere is given by

$$F_b = \frac{2\pi \Delta\rho g R^3 \theta_g}{3}, \tag{3}$$

where R is the channel radius, θ_g is the gas-filled volume fraction, and $\Delta\rho$ is the difference in density between resident and invading fluids. The liquid–gas surface tension restrains growth with a force F_s

$$F_s = 2\pi R \sigma \theta_g. \tag{4}$$

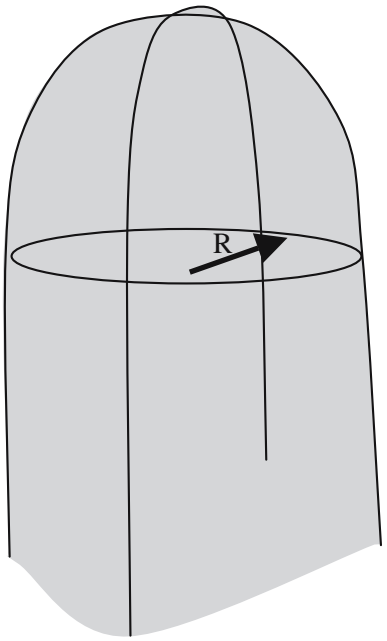

Figure 1. Schematic of buoyant channel geometry with the hemisphere above the circle of radius R imposing a buoyant driving force sufficient to elongate the gas–liquid interface which constitutes the cylindrical walls of the channel.

Balancing these and solving for R we find

$$R = \sqrt{\frac{3\sigma}{\Delta\rho g}}. \tag{5}$$

Using a value of 72.75 dynes/cm for the surface tension between air and water, and 1 gr/cm^3 as the contrast in densities, the predicted radius of the gas channel is 0.4 cm. As the data presented will show, this media-independent value is found to be an excellent approximation for the range of sand grades employed in our experiments. This is consistent with the experimental values from Elder and Benson (1999) that lie between 3 and 8 mm. This dimension also provides physical footing for the observation of previous researchers that in water-filled media with pore spaces greater than 4 mm, gas moves in the form of isolated bubbles; buoyant forces are sufficient to overcome surface tension forces with bubbles of dimension smaller than the inter-granular space. Channel forms arise when the gas filled regions span many pore spaces.

In this case the gas stream is not generally free to pinch off due to hysteresis in the pressure-saturation relationship for the unsaturated

region: the gas pressure would have to drop significantly for the media to re-saturate, which is not expected in a growing plume.

2.2. CONTINUUM SCALE FLOW

We now consider the processes that are important across domains much larger than the channel size (i.e., > 1 cm, but still less than a meter), in particular issues of the path a channel follows and how many channels should arise for a given rate of injection. For this paper we do not consider compressibility effects, though they can be significant as the invasion extends across many meters. Compression changed the volume of invasion, the viscosity of the invading gas, and the mean free path length of molecular movement. These changes, though influential in the overall size and velocity of invasion at the many-meter scale, do not alter the underlying local morphology of the invasion process which is of primary interest to this paper. From this perspective we assume that the gas density and viscosity are sufficiently constant locally for the system to be described with their values taken as constant to understand processes that control gross plume morphology. Clearly when applying these concepts to the field, compressibility would need to be included to obtain accurate predictions. However, the point of this paper is to provide a geometric framework for local plume development.

Thus for locally constant density (incompressible) gas injection, for any gas-filled volume flow will follow the usual form of Darcy's law

$$Q = -\frac{\kappa A}{\mu}\frac{\mathrm{d}P}{\mathrm{d}r}, \tag{6}$$

where Q is the vector mass flux of air under the local potential energy gradient $\mathrm{d}P/\mathrm{d}r$, A is the area of pores and grains through which flow is passing, μ is the dynamic viscosity of the gas, κ is the intrinsic gas permeability of the media at the gas saturation θ_g, encountered by gas-invaded media. We will simplify the system by not considering Klinkenberg slip-boundary and pressure effects, which would be expected to increase the intrinsic permeability by up to a factor of two due to the breakdown in the no-slip boundary condition in the case of a gas (Klinkenberg, 1941). If in the field sparging is undertaken more than about 10 m below the water table, that is at pressures approaching standard atmospheric pressure, these effects will be significant, and must not be ignored. It is important to consider the implications of the fact that the invasion process described here is one of discrete nearly fully gas filled channels of flow rather than smoothly varying volumetric gas contents as would be represented in a continuum model of multiphase processes. Since the gas fills the largest pores within a channel, that the gas permeability where gas is present will

be well approximated by the gas-saturated value. This concept is quite distinct from the continuum approach used to describe gas sparging (e.g., McCray and Falta, 1996), wherein subtle changes in gas saturation are highly influential to local gas permeability. One particular manifestation of this difference is the predicted variation in pressure in the resident fluid. In the channel formulation, once the channel is formed, the geometry of the system is fixed, and the resident-fluid filled pores are now hydrostatic in their pressure distribution. On the other hand, in the continuum description a constitutive relationship is postulated that stipulates a resident fluid capillary pressure that is dictated by the invading gas content. In addition, in the continuum description the permeability that the invading fluid experiences is a strongly non-linear function of the gas content, whereas in the channel description the gas permeability within a channel is to good approximation constant, and will generally be nearly that of gas-filled permeability.

In the immediate vicinity of the injection point there may be a region in which pressure gradients due to viscous resistance to the high imposed near-injection flow significantly exceed the energy gradient from buoyancy. This is here referred to as the "near" injection region, while "far" from the point of injection the flow and gas pressure will no longer be affected by the injection and will instead be controlled by buoyant and hydrostatic forces (Figure 2).

2.2.1. *Far Source Region*

Consider the gas pressure profile in the far region along an already formed stable gas channel that travels from the source to the upper boundary (Figure 2). The pressure distribution in the static and well-connected water phase is hydrostatic in the vertical direction. Since the gas–liquid system is at equilibrium, the gas pressure along the vertical gas–liquid boundary of a channel will be equal to that of the water plus the effective value of P_c (which is effectively constant for a homogeneous media). Hence, the magnitude of the vertical gradient driving gas movement is identically the hydrostatic gradient. Knowing the gradient provides a simple method to estimate of the total cross sectional area of flow for a given mass flux rate and permeability. If air is injected at rate Q, then from Darcy's law for the gas phase, Equation (6), we have for the far plume region

$$Q = -\frac{\kappa A \Delta \rho g}{\mu}, \tag{7}$$

where A is the total cross sectional area of a horizontal slice through the collection of upward flowing gas channels with the density contrast between resident and invading fluids being $\Delta\rho$ (note that the injected

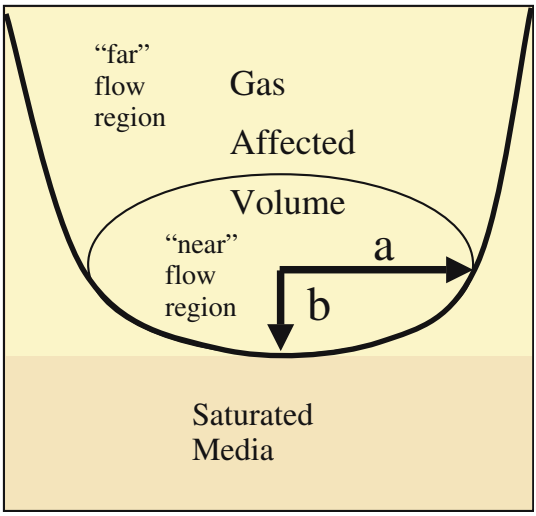

Figure 2. Schematics of the near and far flow regions relative to the point of injection. Near flow represents the region where viscous dissipation driven by gradients in gas pressure flow are in excess of buoyant energy gradients, while in the far flow region buoyant energy gradients are greater than those of gas pressure gradients. The gas affected volume in the near flow region is governed by continuum constitutive relationships in which liquid content is a function of gas pressure, while in the far flow region the flow follows channels that leave portions of the medium completely saturated with a continuous hydrostatic liquid phase.

gas is still taken as approximately incompressible). Taking the value of permeability, κ, at complete gas saturation, κ_{sg}, will provide a reasonably tight lower bound on the cross sectional area of gas flow under unit gradient flow, A_{ug}

$$A_{ug} \geqslant \frac{Q\mu}{\Delta\rho g\kappa_{sg}}. \tag{8}$$

The remarkable feature of the far flow regime is that the predicted cross-sectional area of flow is unaffected by the particular geometry of the channels the gas plume has followed. As well, this implies that the gas-filled pore space is proportional to the discharge, which is precisely the observation of Lazik *et al.* (2002). As mentioned above, for air invading a water filled aquifer, for each 10 m of vertical movement the volume of the gas will double due to compression, which would linearly increase the cross-section of flow. For low rates of flow where channels have not merged, using (5) taking each channel's area to be πR^2 and (8), the number of channels of vertical gas flow N will be on the order of

$$N \approx \frac{Q\mu}{3\pi\sigma\kappa}. \tag{9}$$

The next issue we consider is the horizontal spread of gas channels. In the aquifer far from the point of injection in the horizontal plane, the growth of the plume will be generally upward, with random side-to-side displacements as the channels follow the path of largest adjacent connected pores. The probability of a channel moving in any given lateral direction is equal. To predict the spread of the stands, we desire the probability distribution for position in the horizontal plane as a function of vertical distance from the point of injection. Given that the net lateral displacement is a summation of a number of independent isotropic lateral displacements, by the central limit theorem we conclude that the probability distribution will be Gaussian for any given channel. The standard deviation, SD, of lateral displacement, will be proportional to the square root of the number of pores explored, thus to the square root of the vertical distance the channel has traveled from injection. It is satisfying that the parabolic form of plume development which has been observed (e.g., Ji *et al.*, 1993) is obtained (Figure 3a) based on these simple probabilistic considerations.

We may further note that the full plume of air paths is the sum of a large number of realizations of channels of gas each of which is normally distributed arising from a line source (two-dimensions) or circular source (three-dimensions) described in (8) and (9) (Figure 3b). Assuming for the moment that the source strength of air from the line or circular sources are constant, the sum of the resulting air-streams will follow an error-function distribution in the two-dimensional case, and in the three-dimensional case

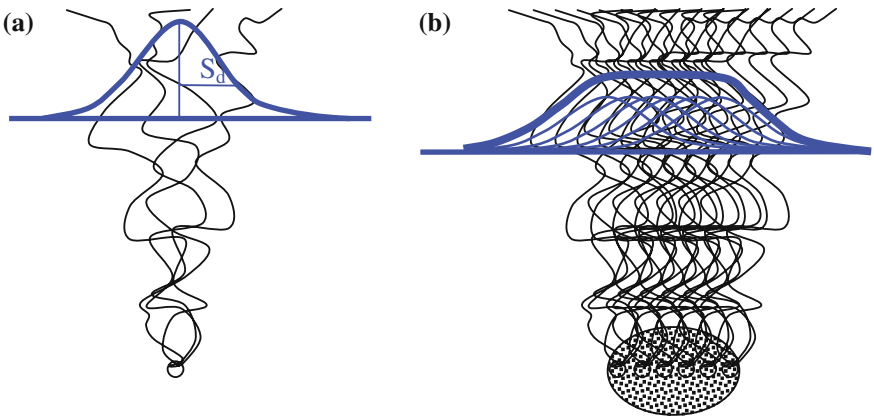

Figure 3. Diagram of the geometry of stands of flow from a point injection. In (a) the injection is mild enough to have the near-field flow be minimal, resulting in purely parabolic growth due to random movement as the channels proceed vertically. In (b) the effects of a significant radial near-source flow is shown, wherein the lateral distribution of gas would be expected to be more closely approximated by superimposed Gaussians.

the error function-like solution, as provided by Leij *et al.* (1991) in their Equation (37).

To this point we have not discussed the role of viscosity on channel growth. The behavior of invasion in porous media is largely independent of viscous effects until the capillary number, C_a (where $C_a = \mu v/\sigma, \mu$ is the viscosity of the resident fluid, and v is the characteristic velocity of the invasion front), exceeds 10^{-4} (Frette *et al.*, 1994). Inspection of Frette *et al.*'s data shows that the smoothing at the 10s of pores scale occurs at much higher capillary number, closer to $C_a = 10^{-2}$. At lower capillary numbers the invasion becomes more complete, but the leading edge of the invasion is still highly serrated. In our case, the channels are already smoothed by Bond Number considerations, and so Capillary Number effects would only be expected when the channel width was less than the smoothing scale due to viscous effects. In the case of water being the non-invading fluid, we may calculate explicitly the critical velocity of about 10 cm/sec, which is beyond the hydraulic conductivities expected for systems with Bond numbers below 1 (which for water suggests a pore size of less than 0.3 cm), where channel behavior is found. Taking the specific flux divided by the volumetric gas content, q/θ_g, to be the invasion velocity, and using the fact that the flow is driven by a unit gradient in the gas phase, the threshold intrinsic permeability may be computed above which viscous forces will be significant to be $\kappa > 10^{-4}\sigma$ which is typically satisfied by media of sand or finer texture, but may be violated for gravels, where bubble-form rather than channel invasion will occur.

2.2.2. *Near Source Region*

It is natural to define the near flow regime to be the region surrounding the point of injection with gas flow area less than A_{ug}. Since the area of flow is less than that required to carry the gas under hydrostatic gradients, it follows that in this region flow must be driven to a significant degree by the pressure supplied by injection. In locally homogeneous media, since the system is driven primarily by gradients in gas pressure, the flow will be radially symmetric We estimate the scale of the near flow regime by computing the radius of a sphere having surface area of A_{ug}. From this perspective we expect the linear scale of this region in three-dimensions, R_{3d}, to be,

$$R_{3d} \approx \sqrt{\frac{Q\mu}{4\pi\,\Delta\rho g\kappa}} \tag{10}$$

and if constrained to a two-dimensional system of thickness T,

$$R_{2d} \approx \frac{Q\mu}{\Delta\rho g\kappa T}. \tag{11}$$

Any viscous resistance to invasion would smooth the invasion front, which would not affect these results which apply after steady flow has been established. Noting that we have drawn the boundary between near and far field flow as that where the energy gradients from buoyant and pressure forces are equal, we can estimate that the lateral near field will be roughly twice as wide as it is deep, thus being perhaps better described below the injection point as an ellipsoid rather than a hemisphere. In this case, we may take the ellipsoid to be symmetric in the horizontal plane and with width, a, twice that of the depth, b. Unfortunately there is no closed form expression for the surface area of a three-dimensional ellipsoid, nor for the perimeter of a two-dimensional ellipse. However, these may be estimated closely enough for our purposes. For the circumference, c of a two-dimensional ellipse the approximation of Euler (1778) is sufficient, where $c \approx \pi\sqrt{2(a^2+b^2)}$. With $a=2b$, this yields $c \approx \pi b\sqrt{10} \cong 3.16\pi b$, about 37% smaller than would have been predicted if one had used the major radius of the ellipse as indicative of a circular region of influence. The surface area of an ellipsoid of rotation about its minor axis, s, is given by the exact expression $s = 2\pi b^2\left[1+\frac{a}{b}\frac{\arcsin(e)}{e}\right]$ where $e=\sqrt{1-b^2/a^2}$ (Granville *et al.*, 1941). With $a=2b$ we find $s=1.71\pi a^2$, which is only 15% different than the area estimate obtained using the spherical assumption. Hence, from this point forward we will simply consider the spherical case, since the level of predictive accuracy is consistent given the assumptions and the homogeneous character of natural media.

3. Experimental Confirmation

To test these predictions we compare them to data from the literature as well as experiments that we carried out. Our experiments consisted of replicated trials in two-dimensional 50 cm tall, 50 cm wide, and 1 cm deep glass-faced slabs of four textures of water-saturated Miller-similar sands (Schroth *et al.*, 1996; Niemet and Selker, 2001). Air was regulated and run through a 1 m column of damp sand to bring it to full vapor saturation, and passed through a digital mass flow meter (Aalborg, Orangeburg, NY, model GFM17 0-15 SLP) before entering the chamber through a fully-penetrating 1 cm diameter sparging stone at pressures always less than 0.2 Bar. The porous medium was held in place on the upper boundary by a manifold consisting of a 3 cm deep acrylic sheet with 0.5 cm perforations covered with a coarse wire mesh to retain the sand. Flow was increased stepwise, waiting for at least 5 minutes to assure steady state between increments of flow. Images of the gas flow were collected using a computer-based video frame grabber from an SVHS color video camera. Measurements were made of the depth of gas entry below the point of injection and the

width of the gas penetration at the depth of injection from these images (Figure 4). Channel flow was prominent in all sands tested with the size of the channels being consistent with the predicted 8 mm diameter. This is somewhat at odds with the predictions of Clayton (1998) who states that channel flow does not occur in fine and medium sands. Close inspection of Claytons claims finds them to be based on a concept that there could only have been channel flow if the degree of saturation was below some threshold (taken to be on the order of 10% volumetric). What we see in our experiments that as flow increases channels fill the pore space evermore completely, eventually obscuring the form of the displacement process, but that in all cases the channels are present and of the same size, as indicated by our theoretical development. Notably, our 40/50 sand has properties that would place it in Clayton's (1998) non-channel invasion category, but in all but the very highest flow rate, the right-hand column of images of Figure 4 clearly shows the channels which built up the desaturated region for this finest sand texture.

The predictions of channel dimensions are well supported by the data of Chen *et al.* (1996) in their Figure 1 where CAT scan data shows channels of 1 cm diameter making up the entire flow regime. Elder *et al.* (1999) also provide excellent channel width data. In their material with 2 mm mean grain size the channels were verging on bubble-form rather than channels, and had diameters averaging 3 mm. In their tests of media of 0.2 mm mean grain size the diameters were found to be 7 mm, again fitting quite well with the predictions of Equation (5).

The experiments confirmed the general observations of Ji *et al.* (1993) of a parabolic plume shape, although clearly the channels define this shape only in a probabilistic sense, with many experiments having single channels of gas percolating further laterally than could be proscribed by a strict parabolic outer bound. As noted above, the gas pressure in the experiments of Ji *et al.* (1993) and our own are subject to gas expansion over the height of the chamber, which gives rise to a net increase in gas volume with elevation. Since these experiments had gas raising less than 1 m, this effect would have only lead to a 10% increase in volume, which is below the level of concern in our analysis.

The relationship between the near injection radius and vertical-to-lateral geometry matched the predictions of Equation (11) very well, and the suggestion that the width of the near zone would be twice the depth (Table I; Figures 5 and 6). Prediction of the specific number of channels of gas were not verified due to the difficulty of discriminating between channels in these small experiments, where many of the channels still overlapped before leaving the short flow path provided in the chamber.

To test the predicted near-source results further we consider several data sets from the literature. Semer *et al.* (1998) provide a very useful

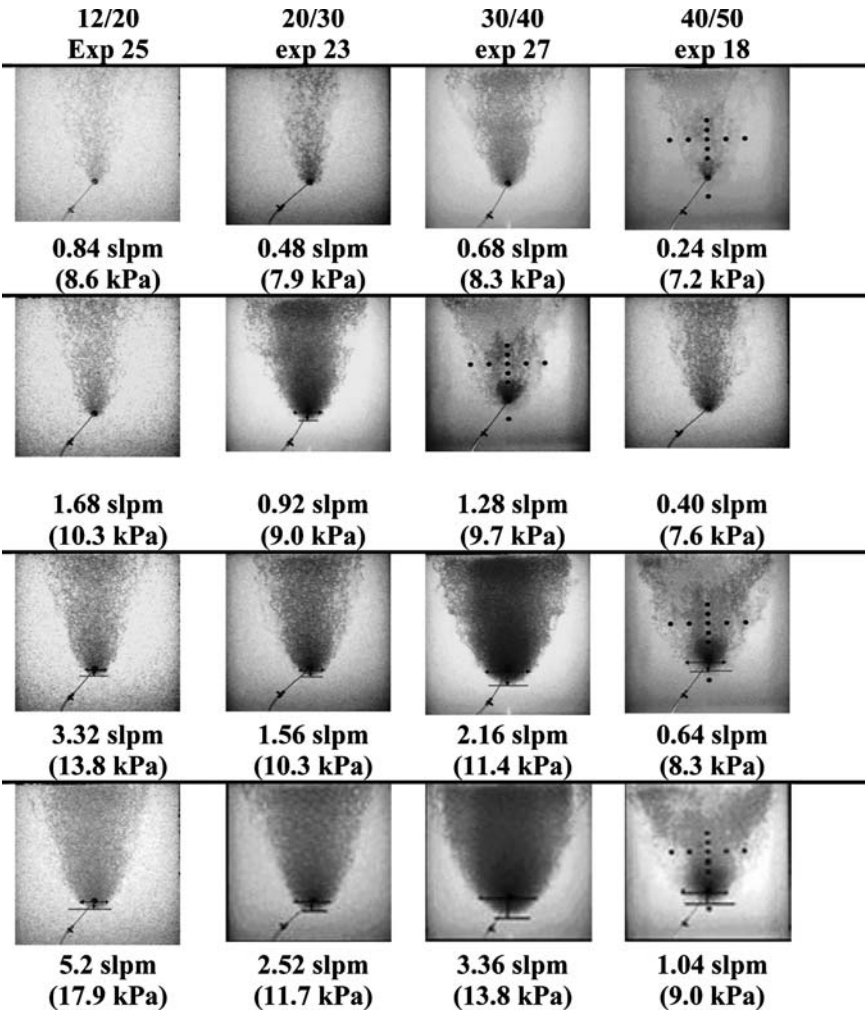

Figure 4. Selected images from two-dimensional injection experiments with flows measured in standard liters per minute (slpm), and injection pressures noted in parentheses. Vertical columns of images are from sequential flow rates, with each column from a particular sand texture. Injection rates increase from top to bottom, reporting both the mass injection rate and back-pressure required to achieve this flow rate. The lowest horizontal lines indicated measured depths of near flow depth of gas penetration, b, while the width of lines through the point of injection represent measured values of a (see Figure 2).

set of data. These authors ran a gas injection into medium gravel at 10 sequentially increasing heads in a chamber 28 cm tall, 40.6 cm wide, and 10 cm deep. Although mass flow rate was not reported, the injection pressure and vacuum applied to the experiment surface were. Assuming a linear relationship between head drop and flow, Equation (11) would

Table I. Geometric results of sparging experiments carried out in 1-cm chambers

Sand	Flux (l/min)	a_{exp} (cm)	a_{pred}(cm)	Ratio a_e/a_p	Ratio b_e/a_e
12/20	5.2	2.1	2.5	0.84	2.0
12/20	3.32	1.6	1.6	0.98	2.0
20/30	1.56	1.9	1.5	1.25	1.9
20/30	2.52	2.3	2.4	0.94	2.4
30/40	1.28	2.3	2.1	1.11	1.7
30/40	2.16	3.6	3.5	1.04	1.6
30/40	3.36	5.1	5.4	0.94	1.6
40/50	0.64	2.4	2.1	1.12	2.2
40/50	1.04	3.4	3.5	0.99	2.0

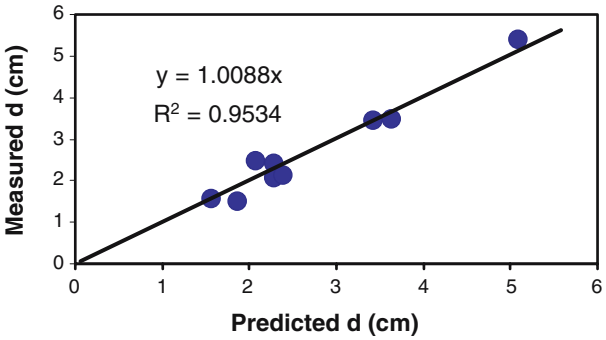

Figure 5. Predicted and observed near-source radial flow diameters for the tests summarized in Table I.

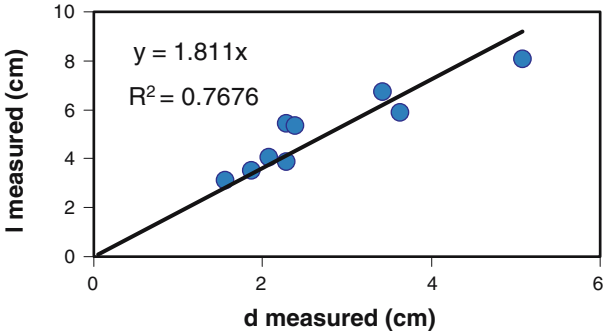

Figure 6. Predicted versus measured near-field plume width for two-dimensional flow for the experiments listed in Table I.

predict a linear relationship between near-injection radius and total applied head. At total heads of 29.4 kPa and lower, the plume had a constant width that was just sufficient to span the chamber width of 10 cm, and this dimension did not change as a function of head. At these low flow rates we can assume that the near injection radius was negligible compared to the random spreading due to vertical migration, which is supported by the diagrams provided by Semer *et al.* (1998) in their Figure 4. In our conceptualization, the near-injection spreading should add linearly to this migration-spreading, so to estimate the near-injection spreading we simply subtract 10 cm from the observed final width. Semer *et al.* (1998) continued increasing their injection rates until the pattern nearly filled the entire width of the chamber, which at the highest flow rates artificially limited the pattern spread. Thus, using all but the highest three data points where boundary effects were expected, and accounting for the 10 cm migration spreading, Equation (11) fits the data with $r^2 = 0.99$, supporting the concept of near-source spreading due to viscous dissipation presented here (Figure 7).

Semer *et al.* (1998) also present data from three-dimensional experiments where the width of the plume was measured as a function of the distance upward from the source. In the case of the sand experiments, the flow rates were, unfortunately for our purposes, chosen to be high enough for the near-source predicted radius to be greater than the depth of the chamber. However, in the fine gravel study, the flow rates were somewhat lower.

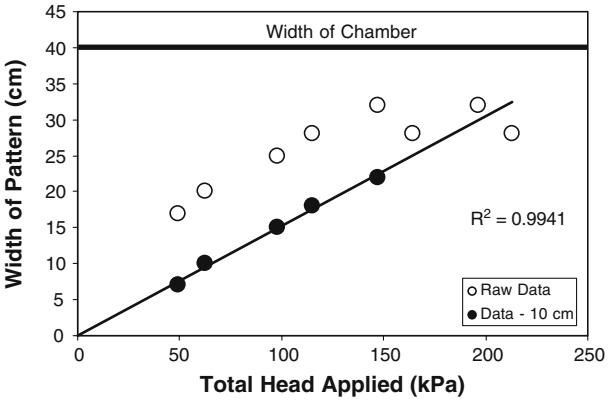

Figure 7. Re-analysis of Semer *et al.*'s (1998) data presented in their Figure 4 to asses the prediction that near-field flow should scale linearly with flux in two-dimensional systems. The pseudo-two dimensional chamber had a depth of 10 cm, which was subtracted from the observed plume width, since a plume of 10 cm width would be observed as a line of zero width on the glass wall of the chamber. Similarly, reported widths within 10 cm of the width of the chamber were likely affected by the constraints of the boundaries.

This combined with the much higher permeability, leading to predicted near-source radii of approximately 4 cm from Equation (10), is less than the observed spreading, indicating that random vertical spreading should also be expected. Our random path concept suggests that the width of the plume should increase with the square root of the vertical distance from the source, as found (reproduced here as Figure 8). This is in fact in marked contrast to Semer *et al.*'s (1998) conclusions, which are that the plume width "stabilized after 15 cm depth", a discrepancy with significant practical ramifications with respect to the volume treated by a sparging system.

Hein *et al.* (1997) present a rich data set to compare to theory. A 120 cm diameter cylindrical tank was filled with silica sand to a depth of 65 cm. Four experiments were carried out, with air sparged into the system at 62, 187, and 283 lpm (two tests). The authors measured the flux as a function of distance from the center. Using their values of permeability, the radii of near-source radial flow (Equation (9)) are estimated for these flow rates to be 3.9, 6.8, and 8.3 cm. With these values, we may estimate the radial distribution of air emissions using the solution of Liej *et al.* (1991, Equation (37)), as implemented in STANMOD, with the data fit to the model using the inverse model tool (Simunek *et al.*, 1999). All the experiments should plot onto the same curve if the estimated near-source radii are subtracted from the actual radial distance, and the observed fluxes are divided by the injection rate. The data, thus prepared, show remarkable fit to the theory, and have quite consistent fitted channel dispersivities (proportional to S_d) between experiments (Figure 9). This is quite in contrast to the model predictions of Hein *et al.* (1997) themselves, wherein there model under-predicts flux for all the data near the well, and over-predicts flux

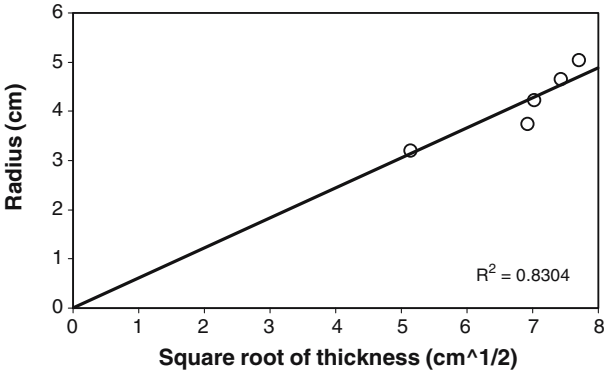

Figure 8. Data from Semer *et al.*'s (1998) Figure 6 for fine gravel testing the relationship between plume width and vertical rise in their three-dimensional tank experiments.

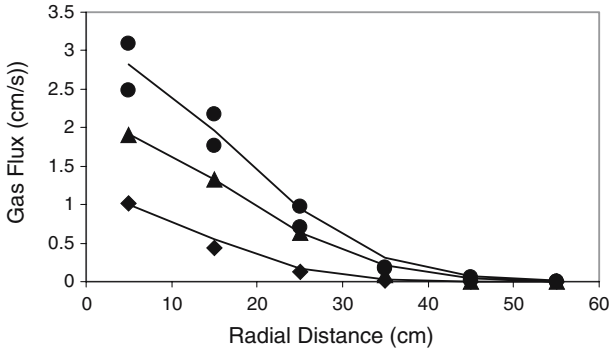

Figure 9. Fit disk-source dispersion using STANMOD to the experimental data of Hein *et al.*'s (1997) Table II, with source radii computed using Equation (11). Diamonds are from the 62 lpm test; triangles from the 187 lpm test; and circles from the two 283 lpm tests. Fitted dispersivities were 2.1, 3.7, and 3.7 cm respectively.

for almost all points far from the well. Their model, as described fully in McCray and Falta (1996), is not consistent with the patterns of flow observed in the experimental studies. They assume a gas-liquid continuum whereas the experiments show discrete channels of gas separated by saturated hydrostatic media. This dichotomy is illustrated directly by McCray and Falta (1996, Figure 1), and is quantified in their Figure 7 where a water-phase pressure gradient is shown from the center of the injection, which would not occur in the case of an assemblage of discrete channels of gas. Thus, it appears that the model presented and employed in those papers is faulty in concept for this system except for the near-field flow region. These contrasting concepts of flow are well described by Clayton (1998) (see Clayton's figure 12).

4. Conclusions

The central features of the proposed model are: viscous effects of the resident water are negligible for gas invasion of a water-filled sand textured medium; above the far from injection region the horizontal cross-sectional gas-filled area will increase linearly with height due to decreasing hydrostatic forces; the area of the gas plume being affected first by the injection rate in a near-injection radius; and, the span of the gas plume expanding in a diffusion-like manner as the channels randomly advance upward. Quantitative expressions based on these features are presented.

The key characteristics of injected gas movement in a porous media acted upon by gravity are that the flow is horizontally radially dominant when gas pressure gradients are in excess of the hydrostatic gradient, and vertically dominant when displacement exceeds lesser gradients. In the domain of

vertical movement, the gas flow geometry takes on three possible forms (bubble, dendritic, and channel) depending on the Bond number, with bubbles being found in water-filled media with pore size greater than about 4 mm, channels for media with pores smaller than 0.5 mm, and dendritic forms between these two limits. Previous theoretical studies have focused primarily on dendritic and bubble movement, while here the characteristic behavior of channels is most closely considered. Channels are shown to be the expected form for water filled media with texture of sand or finer, and have a characteristic dimension of about 4 mm. The widely observed qualitatively parabolic shape of observed gas plumes is proposed to be a simple ensemble outcome of the sum of many random lateral displacements of the many independent channels of gas. We suggest that probability distribution for lateral position of any single channel is Gaussian with a variance that grows with the square root of total displacement. This model predicts gas distributions consistent with numerous published data sets, as well as the data obtained in the experiments described here. Previous continuum models of gas movement do not capture this characteristic, as is apparent when previous results of these models based on standard continuum constitutive relations are considered with these observations in mind.

Several of the suppositions of our analysis should be kept in mind. We assume that the medium is non-deforming throughout the invasion. We further treat the gas as locally invariant in density, though where compressibility would be significant we have noted in principle how these effects would be accounted for. We have also assumed the medium is homogeneous. On this count application of our results to naturally occurring formations must be undertaken with great care. Extensive natural sand-textured materials are deposited in a sequence of high energy events (e.g., wind storms and floods). Such events are characterized by highly variable energy, thus depositing finer and coarser beds as the turbulent energy allows different sizes to settle or be suspended. This intrinsically layered character leads to dramatic lateral flow patterns as these layers create capillary breaks that impede gas movement. Thus, while in the laboratory we can achieve vertical uniformity, this is not generally expected in nature. Despite this important limitation, the results presented are likely to be helpful for qualitative description, and in cases of man-made systems such as enclosed granular reactors, and engineered systems found in mining and construction sites. Further research on these processes is necessary, with several recent fruitful efforts published (e.g., van Dijke and van der Zee, 1998; Peterson *et al.*, 2001; Reddy and Adams, 2001).

Many of the observations made here can be applied to other fluid-invasion processes that might occur between immiscible liquids (e.g., TCE and water) that might have very different viscosity, density, and flow rate behaviors. The translation to these extensions could likely be made since all the

key results are written in terms of basic physical properties, though care is necessary when the contact angles differ from that of the air–water system considered here, among other potential complications.

References

Baldwin, C. A. and Gladden, L. F.: 1996, NMR imaging of nonaqueous-phase liquid dissolution in a porous medium, *AIChE J*. **42**, 1341–1349.

Brooks, M. C., Wise, W. R. and Annable, M. D.: 1999, Fundamental changes in in-situ air sparging flow patterns, *Ground Water Monit. Rem*. **19**(2), 105–113.

Chaouche, M., Rakotomalala, N., Salin, D., Xu, B. and Yortsos, Y. C.: 1994, Invasion percolation in a hydrostatic or permeability gradient: experiments and simulations, *Phys. Rev. E*. **49**(5), 4133–4139.

Chen, M.-R., Hinkley, R. E. and Killough, J. E.: 1996, Computed tomography imaging of air Sparging in porous media, *Water Resour. Res*. **32**(10), 3013–3024.

Clayton, W. S.: 1998, A field and laboratory investigation of air fingering during air sparging, *Ground Water Monit. Rem*. **18**(3), 134–145.

Conrad, S. H., Wilson, J. L., Mason, W. R. and Peplinski, W. J.: 1992, Visualization of residual organic liquid trapped in aquifers, *Water Resour. Res*. **28**(2), 467–478.

Culligan, Patricia J., Barry, D. A., Parlange, J.-Y., Steenhuis, T. S., Haverkamp, R.: 2000, Infiltration with controlled air escape, *Water Resour. Res*. **36**(3), 781–785.

Dror, I., Berkowitz, B. and Gorelick, S. M.: 2004, Effects of air injection on flow through porous media: observations and analyses of laboratory-scale processes, *Water Resour. Res*. doi:10.1029/2003WR002960.

Elder, C. R. and Benson, C. H.: 1999, Air channel formation, size, spacing, and tortuosity during air sparging, *Ground Water Monit. Rem*. **19**(3), 171–181.

Euler, L.: 1778, De reductione linearum curvarum ad arcus circulares, *Nova Acta Acad. Petropol*. **7**, 58.

Frette, V., Feder, J., Jøssang, T. and Meakin, P.: 1992, Bouyancy-driven fluid migration in porous media, *Phys. Rev. Let*. **68**(21), 3164–3167.

Frette, V., Feder, J., Jøssang, T., Meakin, P. and Jørgen Måløy, K.: 1994, Fast, immiscible fluid–fluid displacement in three-dimensional porous media at finite viscosity contrast, *Phys. Rev. E*. **50**(4), 2881–2890.

Fry, V. A., Selker, J. S. and Gorelick, S. M.: 1997, Experimental investigations for trapping oxygen gas in saturated porous media for In situ bioremediation, *Water Resour. Res*. **33**(12), 2687–2696.

Granville, W. A., Smith, P. F. and Longley, W. R.: 1941, *Elements of the Differential and Integral Calculus*, Rev. Ed. Boston: Ginn and Co., 280.

Hein, G. L., Gierke, J. S., Hutzler, N. J. and Falta, R. W.: 1997, Three-dimensional experimental testing of a two-phase flow-modeling approach for air sparging, *Ground Water Monit. Rem*. **17**(3), 222–230.

Hirsch, L. M. and Thompson, A. H.: 1994, Size-dependent scaling of capillary invasion including buoyancy and pore size distribution effects, *Phys. Rev. E*. **50**(3), 2069–2086.

Imhoff, P. T., Jaffe, P. R. and Pinder, G. F.: 1994, An experimental study of complete dissolution of a nonaqueous-phase liquid in saturated porous media, *Water Resour. Res*. **30**(2), 307–320.

Ji, W., Dahmani, A., Ahlfeld, D. P., Lin, J. D. and Hill, E.: 1993, Laboratory study of air sparging: air flow visualization, *Ground Water Monit. Rem*. **13**(4), 115–126.

Klinkenberg, L. J.: 1941, *The Permeability of Porous Media to Liquids and Gases. Drilling and Production Practice*, Am. Petro. Inst., NY, pp. 200–213.

Krauss, G., Lazik, D. and Geistlinger, H.: 2003, Gas Sparging for bioremediation: Experimental investigations of gas phase distribution, in: Proceedings of the 2nd European Bioremeidation Conference Chania/Kreta, Greece. March 30–April 7, 2003.

Lazik, D., Geistlinger, H., Krauss, G., Beckmann, A. and Schrimer, M.: 2002, Untersuchungen zum Strömungsverhalten und zur Lösungskinetik von Gasen im Mehrphaensystem "Aquifer." *Grundwasser* (3), 146–155.

Leij, F. J., Skaggs, T. H. and van Genuchten, M.Th.: 1991, Analytical solutions for solute transport in three-dimensional semi-infinite porous media, *Water Resour. Res*. **27**(10), 2719–2733.

Lohse, D.: 2003, Bubble Puzzles, *Phys. Today* **2**, 36–41.

McCray, J. E. and Falta, R. W.: 1996, Defining the air sparging radius of influence for groundwater remediation, *J. Contam. Hydrol*. **24**, 25–52.

Niemet, M., Selker, J. S.: 2001, A new method for quantification of liquid saturation in 2-d translucent porous media systems using light transmission, *Adv. Water Resour*. **24**, 651–666.

Peterson, J. W., Murray, K. S., Tulu, Y. I. and Peuler, B. D.: 2001, Air-flow geometry in air sparging of fine-grained sands, *Hydrogeol. J*. **9**, 168–176.

Reddy, K. R., Semer, R., Adams, J. A.: 1999, Air flow optimization and surfactant enhancement to remediate toluene-contaminated saturated soils using air sparging, *Environ. Manage. Health* **10**(1), 52–63.

Reddy, K. R. and Adams, J. A.: 2001, Effects of soil heterogeneity on airflow patterns and hydrocarbon removal during in situ air sparging, *J. Geotech. Geoenviron. Eng*. **3**, 234–247.

Reddy, K. R. and Tekola, L.: 2004, Remediation of DNAPL source zones in groundwater using air sparging, *Land Contam. Reclamation* **12**(2), 67–84.

Roosevelt, S. E. and Corapcioglu, M. Y.: 1998, Air bubble migration in a granular porous medium: Experimental studies, *Water Resour. Res*. **34**(5), 1131–1142.

Schroth, M. H., Ahearn, S. J., Selker, J. S. and Istok, J. D.: 1996, Characterization of Miller-similar silica sands for laboratory hydrologic studies, *Soil Sci. Am. J*. **60**, 1331–1339.

Semer, R., Adams, J. A. and Reddy, K. R.: 1998, An experimental investigation of air flow patterns in saturated soils during air sparging, *Geotech. Geol. Eng*. **16**, 59–75.

Simunek, J., van Genuchten, M. Th., Sejna, M., Toride, N. and Leij, F. J.: 1999, The STANMOD computer software for evaluating solute transport in porous media using analytical solutions of convection-dispersion equation. Versions 1.0 and 2.0, IGWMC - TPS - 71, International Ground Water Modeling Center, Colorado School of Mines, Golden, Colorado, 32 pp.

van Dijke, M. I. J. and van der Zee, S. E. A. T. M.: 1998, Modeling of air sparging in a layered soil: Numerical and analytical approximations, *Water Resour. Res*. **34**(3), 341–353.

Xu, B. and Yortsos, Y. C.: 1998, Invasion percolation with viscous forces, *Phys. Rev. E*. **57**(1), 739–750.